The ramp widths of high-Mach-number, quasi-perpendicular collisionless shocks

J. A. Newbury and C. T. Russell

Institute of Geophysics and Planetary Physics, University of California Los Angeles

M. Gedalin

Department of Physics, Ben-Gurion University, Beer-Sheva, Israel

Abstract. The shock ramp is traditionally defined as the narrow region over which the magnetic field primarily jumps from upstream to downstream conditions. Although narrow in comparison to other features in the shock profile, the ramp plays the most important role in providing the necessary dissipation of the incident solar wind flow. However, its features are not well understood, particularly for shocks observed when the upstream solar wind has a high Mach number and high plasma β. Using the ISEE 1 and 2 spacecraft to measure the spatial scales in supercritical, quasi-perpendicular bow shock profiles, we examine the scale size of the ramp and pay particular attention to features found within the ramp. It is shown that the ramp can usually be characterized by two different scales: (1) a large scale (or global ramp width) within which the main transition from the upstream to downstream magnetic field occurs and (2) a thinner subramp scale which contains steep jumps in the magnetic field magnitude with amplitudes comparable to the overall change in magnetic field at the shock. It is shown that both scales are characteristic of the quasi-stationary shock profile (and are stationary within an ion gyroperiod), which allows for a reliable conversion from measured temporal durations to spatial lengths in the shock profile. In most shocks the global ramp width is 0.4-1 ion inertial lengths (c/ω_{pi}), and the subramp scale is about 0.1-0.2 c/ω_{pi}. We argue that presence of these small-scale, large-amplitude, quasi-stationary structures in the ramp may be important for ion dynamics. An oscillatory behavior of the ramp is also observed in some shocks. Also, the global ramp width and subramp scales show little dependence on upstream parameters: The global ramp scale thins as θ_{Bn} approaches 90°, but not as much as predicted, and there is little overall correlation between ramp scales and either Mach number or β. Future multispacecraft observations of the bow shock will require high-temporal-resolution measurements and close spatial separations to address the problem of shock structure. Present plans for the Cluster mission will provide little data at the close separations needed for such a study.

1. Introduction

The quasi-perpendicular collisionless shock is noted for its thin, structured transition between upstream and downstream regimes. The feature known as the shock ramp is traditionally defined as the narrow region over which the magnetic field experiences its main transition. In this picture the magnetic field increases monotonically in the ramp, generally increasing in strong shocks by a factor of 3-5 [e.g., *Scudder et al.*, 1986a, Figure 1]. Other features of the high-Mach-number shock profile include a wide foot which lies just upstream of the ramp and an even wider overshoot and undershoot region located downstream of the ramp.

It is within the large magnetic field jump at the ramp where the most dramatic changes occur to the incident solar wind plasma. Ions are decelerated and some are reflected back into the solar wind (which result in the foot and overshoot features noted above) [*Sckopke et al.*, 1983; *Burgess et al.*, 1989; *Wilkinson and Schwartz*, 1990; *Gedalin*, 1996]. The ramp is also where prompt electron heating is observed [*Feldman*, 1985; *Scudder et al.*, 1986b; *Thomsen et al.*, 1987; *Schwartz et al.*, 1988]. Though narrow in size when compared with the rest of the shock profile, it is the ramp which plays the most important role in providing the necessary dissipation of the incident solar wind. Knowledge of the scale size of the ramp helps to determine the processes which dissipate the plasma in that region. Despite the importance of the ramp, its basic parameters, especially its width, are not well known. It is the purpose of this paper to explore the features of ramps observed in high-Mach-number, high-β bow shocks, paying particular attention to the complicated features found within the ramp transition.

The ramp width of a low-Mach-number shock is fairly well understood: The effects due to ion reflection and the overall shock energetics are both weak, which results in a simpler magnetic profile. The shock structure is related to a large-amplitude whistler wave which extends upstream as a phase-standing precursor wave train. The thickness of the low-Mach shock ramp width is observed to be on the order of an ion inertial length, c/ω_{pi} [*Farris et al.*, 1993] or within a factor of 2 to the whistler precursor half-wavelength $\pi c \cos\theta_{Bn}/\omega_{pi}\sqrt{M_A^2 - 1}$ [*Mellott and Greenstadt*, 1984]; here, M_A is the Alfvénic Mach number, θ_{Bn} is the angle between the shock normal and upstream magnetic field, and ω_{pi} is the proton plasma frequency. The width of the ramp can also be predicted with reasonable accuracy and be used as a "ruler" with which to measure the spatial scales of the low-Mach shock [*Newbury et al.*, 1997].

There are no statistical analyses of the ramp width for high-Mach-number shocks. As the plasma dissipation processes become more complex, the shock profile becomes more difficult to interpret. In a very detailed analysis of a single bow shock crossing, *Scudder et al.* [1986a] reported the ramp width to be 0.2 c/ω_{pi}, a measurement based on an exponential fit of the foot-ramp transition. Also applying exponential fits to the shock profile, *Russell and Greenstadt* [1979] measured slightly thicker ramps on the order of 0.4 c/ω_{pi} in an initial study of ISEE bow shock observations.

0148-0227/06/$9.00

A study of seven nearly-perpendicular shocks ($\theta_{Bn} > 80^\circ$) by *Newbury and Russell* [1996] found a range of ramp widths (based on a linear fit to the ramp transition) from 0.5-0.8 c/ω_{pi}; however, in one case the ramp width was particularly thin, 0.05 c/ω_{pi} ($\sim$2 c/ω_{pe}). It was postulated that this remarkably thin shock was due to the very perpendicular nature of θ_{Bn}: Finite ion inertia plays no role in exactly perpendicular shocks, but dominates the dispersive structure of slightly oblique shock waves [*Karpman*, 1964]. A thin shock could also be explained in terms of the "shock from a soliton" concept, originally proposed for perpendicular propagation in a cold plasma [*Sagdeev*, 1966]. According to this scenario, the ramp width must be on the order of the dispersion length since the dispersion limits nonlinear steepening. In the perpendicular case this length is the electron inertial length. This concept was generalized to the oblique case [*Kennel and Sagdeev*, 1967], which suggests that the basic ramp scale be $c\cos\theta_{Bn}/\omega_{pi}$. Other approaches to understanding ramp thicknesses in terms of plasma dissipation at the bow shock include the anomalous resistivity induced by the ion-acoustic instability (for low-Mach-number shocks) [*Morse and Greenstadt*, 1976], and steepening and overturning of the shock profile which would result in a steep but nonstationary front (for oblique, high-Mach-number shocks) [*Galeev et al.*, 1988]. None of these approaches has been particularly successful in explaining the observed steepness of the shock ramp.

The common method used to measure the ramp width in a shock observation is to use an exponential fit to the foot-ramp region [e.g., *Russell and Greenstadt*, 1979; *Scudder et al.*, 1986a] or a linear fit of the magnetic field jump in the ramp [*Greenstadt et al.*, 1975; *Newbury and Russell*, 1996]. As we shall illustrate in this paper, these simple approximations provide reasonable descriptions of the region within which the most energetic processes occur, but such fits ignore the finer-scale, large-amplitude substructure commonly observed in the high-Mach-number shock. If, for example, a ramp is not a single monotonic transition but consists of two or more large-amplitude subtransitions, the simple linear fit is misleading. The particle motion and consequent heating and dissipation in the shock layer may be quite different within a single, wide, and monotonic ramp when compared to a ramp with several successive steep, large-amplitude subramps.

In this paper we examine shock scale measurements from a selection of supercritical, quasi-perpendicular bow shocks observed by the ISEE 1 and 2 spacecraft. We use the linear fit to the ramp region, which measures what is hereafter called the "global ramp width." To study subramp scales, we utilize wavelet transforms to locally identify and analyze the steepest gradients found within the global ramp that are also accompanied by large, quasi-monotonic magnetic field increases.

2. The Data Set

The ISEE 1 and 2 mission provides excellent opportunities to measure the fine-scale structure of the Earth's bow shock. The close orbits of the two spacecraft allow for accurate determination of the shock velocity based on the small temporal and spatial separations of each spacecraft's shock observation. With the shock's velocity, the observer may convert the temporal shock profile into a more physically meaningful spatial profile.

Shock crossings are identified from data collected by the ISEE 1 and 2 fluxgate magnetometers [*Russell*, 1978]. Data are filtered to obey the Nyquist criterion and then sampled at a high-resolution rate of either 4 or 16 vectors per second.

In addition to the magnetic field measurements, moments from the plasma distributions measured by the Solar Wind Experiments on ISEE 1 and ISEE 3 [*Bame et al.*, 1978] are used to calculate magnetosonic and Alfvénic Mach numbers ($M_{\rm MS}$ and M_A), plasma β (the ratio of total thermal pressure to magnetic pressure), θ_{Bn} (the angle between upstream magnetic field and the shock normal), and ion inertial length (c/ω_{pi}). The assumption that $\gamma = 5/3$ is taken for the polytropic index in calculations of $M_{\rm MS}$. When electron temperature measurements from ISEE 3 were unavailable (generally, dates before August 16, 1978), the assumption that $T_e = 141,000$ K was made for calculations of β and $M_{\rm MS}$ [*Newbury et al.*, 1998]. Proton beta (β_p) is always based on an observed proton temperature.

In this study we consider quasi-perpendicular shocks with high-Mach-numbers ($\theta_{Bn} > 45^\circ$ and $M_A > 3$). Shock normals are calculated using the magnetic coplanarity assumption, where upstream and downstream states are defined by averaging over several minutes of steady, undisturbed field measurements. To avoid observations where two-dimensional fluctuations on the shock front may be an issue, coplanarity normals were compared with normals determined from an ellipsoidal bow shock model (with an eccentricity of 0.81[*Farris et al.*, 1991]), and only those shocks where normals from both methods agree within 10° were selected. For Mach number calculations, plasma bulk speed is resolved along the shock normal (in the reference frame where the shock front is stationary). The dates, times, and relevant parameters (including proton gyroperiod, $2\pi/\Omega_p$) for the shock observations used in this study are listed in Table 1.

All scale measurements and spacecraft separations reported in sections 4 and 5 are measured with respect to the upstream ion inertial lengths listed in Table 1.

The shock crossings and their corresponding spacecraft positions, separations (normal and transverse to the shock), and velocities are listed in Table 2. Only those shocks with small spacecraft separation along the normal ($20 < \Delta d_{sc,n} < 500$ km) were considered. Cases with extremely small separations were not considered to avoid large relative errors, and cases where spacecraft separations were much larger than 500 km tend to contain significant temporal and/or spatial variations between the ISEE 1 and 2 observations. (One case, on August 13, 1979, has a larger spacecraft separation, but is included here since the two profiles were quite comparable in this instance.)

Velocities ($v_{\rm sh,n}$) are calculated by determining the time separation between shock observations by ISEE 1 and 2 and the spatial separation of the spacecraft in the direction along the shock normal. (This assumes that shock velocity is constant throughout the ISEE 1 and 2 observations of the shock.) Shock observations whose velocities are low are most desirable; the spacecraft will record far more detail in a shock profile where the shock front is moving slowly than one where it speeds across the magnetometer (which has a fixed bandwidth maintained by anti-aliasing filters). Some higher velocity shocks are included in this study to illustrate the effect of shock velocity on observed ramp thickness (see also Figure 1 of *Newbury and Russell* [1996].)

3. The Utilization of Wavelet Transforms

Our goal is to identify sharp gradients with large magnetic field jumps in the shock layer. This is a task which is ideal for wavelet analysis. Identifying such structures "by eye" is exceedingly subjective and quite difficult, especially when there is a large amount of turbulence and wave activity in the shock layer. Cross-correlation analysis, although successful at determining lags between two overall profiles, breaks down at smaller scales, not because smaller scales are not comparable but because turbulence and wave activity obscures those scales. Reducing turbulence by averaging a profile has the unfortunate effect of spreading out any structural gradients in the profile. Cross correlation also tends to fail when multiple spacecraft have different observational viewpoints of the same structure. *Rezeau et al.* [1998] have used an adaptive correlation function, derived from wavelet analysis, to compare multi-spacecraft observations of field aligned currents. In this paper we avoid this difficulty by placing strict limitations on the separation of the ISEE 1 and 2 spacecraft when selecting shock observations for study. We identify similar features and scale sizes in the ISEE 1 and 2 magnetic profiles by a direct comparison of the profiles' wavelet transforms.

The wavelet transform allows one to obtain information about both the scale size and position of a feature within a profile. It utilizes analyzing functions called wavelets, which are localized in

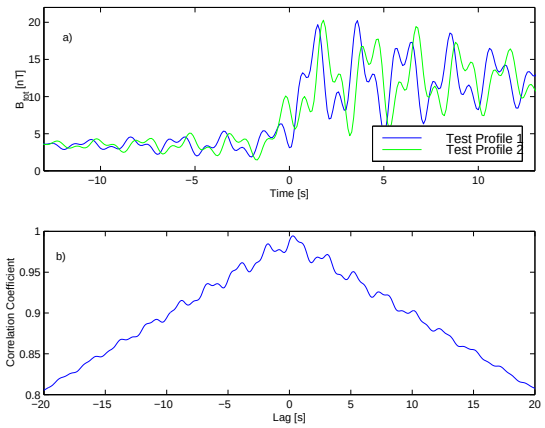

Figure 1. (a) Two test profiles, constructed from a hyperbolic tangent ramp placed at t=0 and two exponentially damped sine waves (with different phases in profiles 1 and 2). (b) Cross-correlation analysis of these two profiles shows that the average lag is zero.

space and play no role when infinitely far away; thus wavelet analysis is performed locally, unlike a Fourier transform, which is inherently nonlocal. The decomposition of scales within a profile is obtained by contracting and dilating the wavelet function over a range of widths before convolving it with the profile. For an overview of wavelet transforms, we refer the reader to the review by *Farge* [1992]. Details on the specific application of wavelet transforms to shock profiles are given by *Gedalin et al.* [1998], whose techniques we follow closely in the present paper. In order to develop a basis with which to interpret transforms in terms of shock structure,

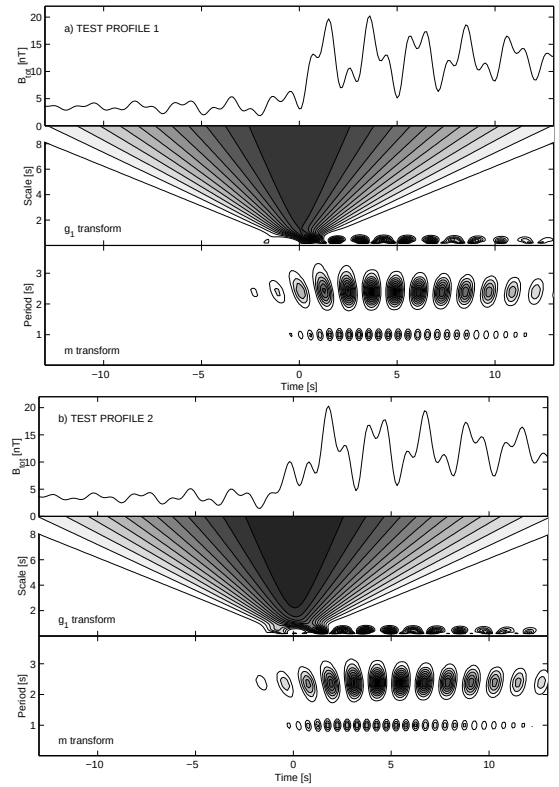

Figure 2. (a) Test profile 1 and its corresponding g_1 and m wavelet transforms. (b) As above, for test profile 2. The wavelet transforms provide additional information about the sharp gradients and wave activity in each profile.

Gedalin et al. [1998] use wavelet transforms created from a variety of model shock profiles with predefined ramp widths and wave activity. The extrapolation of wavelet transforms from model profiles to actual shock observations works well.

The choice of the wavelet function used in the transform is based on one's needs. Generally, the best choice will resemble the desired feature in the profile. In our analysis we apply a wavelet transform based on the first derivative of a Gaussian (hereafter referred to as the g_1 transform). This transform is particularly useful for shock ramp studies because it highlights the steepest gradients with the largest jump in the magnetic field, ignoring the presence of wave activity and turbulence (which tends to obscure more traditional methods of ramp identification). As illustrated by *Gedalin et al.* [1998], the g_1 transform allows the observer to ignore large-amplitude alternating fluctuations, even when superimposed upon large gradients, and instead the observer may focus on the structures which clearly exhibit a nonoscillating character. To examine wave activity, the Morlet wavelet (hereafter the m transform) is a good choice. The Morlet wavelet is simply a monochromatic wave within a Gaussian envelope.

3.1. An Introductory Example

In Figure 1 we present two test shock profiles which are constructed to mimic observed shock profiles. Specifically,

$$B_{\rm tot} = B_0(1 + A_0 C_0) \tag{1}$$

where

$$B_0 = 8 + 4.5\tanh(1.5t) \tag{2}$$

$$A_0 = 0.4\sin(2\pi(t - t_1)/2.4) + 0.25\sin(2\pi(t - t_2)/1) \tag{3}$$

$$C_0 = \exp((3 - t)(t - 1)/150) \tag{4}$$

The only differences between the two test profiles are the phases of the sine waves defined in equation (3): $t_1 = 0.7$ and $t_2 = 0.3$ in test profile 1 and $t_1 = 3.7$ and $t_2 = 2.5$ in test profile 2. (In comparison to a typical bow shock observation, the wave activity is somewhat exaggerated in these model profiles so that we may clearly illustrate the usefulness of wavelet transforms.) The hyperbolic tangent "ramp" (equation (2)) is positioned at $t = 0$ in both test profiles. Visually, the two profiles appear quite different due to the sine waves (which also severely obscure the ramp). Cross-correlation analysis shows that the two profiles do in fact correlate quite well (the maximum correlation coefficient is near 1.0) and that there is zero lag between the two profiles overall (as defined above).

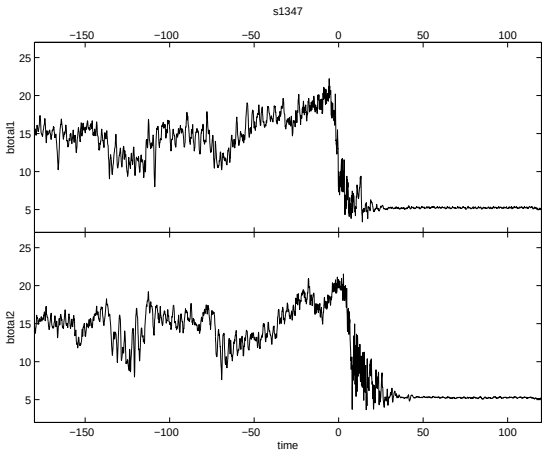

Figure 3. The ISEE 1 and 2 total magnetic field profiles for the shock observed on August 2, 1980, 0858 UT; $\theta_{Bn} = 86°$, $M_{\rm MS} = 3.0$, and $\beta = 0.91$. Time = 0 = 0858:50 UT. This high-Mach-number, quasi-perpendicular shock exhibits the classic foot-ramp-overshoot profile.

When we examine the wavelet transforms of these profiles, additional information can be obtained (Figure 2). As described by *Gedalin et al.* [1998], the contours in the g_1 transform which converge from large to small durations (i.e., scale size) indicate the position of the ramp. In Figure 2, contours converge to $t = 0$ in each test profile. Comparison of the transforms from each profile provides us with the same information as the cross-correlation analysis: The time lag between profiles is 0 s. However, the wavelet transforms provide additional important information: the position of sharp gradients within the profile. Furthermore, it is seen that the g_1 transform allows the observer to ignore wave activity. (There are bumps in the transform at small scales, corresponding to the large amplitude waves, but it is the converging "cones" of contours from large to small scales which indicate a large gradient.) The Morlet transform provides information about wave activity by highlighting periodic structures in a profile and ignoring ramplike gradients. Wave trains are indicated by the periodic "bumps" in the Morlet transform. For these two test profiles, the "bumps" indicate two wave trains at periods of 2.4 and 1 s, respectively (as defined above in equation (3)), and the amplitudes trail off as defined by equation (4). Comparison of the bump positions between the two profiles shows the phase differences as set by the values of t_1 and t_2.

In section 4 we shall apply these wavelet transforms to a variety of high-Mach-number, high-β shock profiles and interpret them.

3.2. "Quasi"-Stationarity

By comparing features highlighted in the wavelet transforms from the ISEE 1 and 2 profiles, one can separate quasi-stationary features from those that are fluctuating. Features in each of the profiles' transforms which "match up" are said to be stationary within the limit of the temporal separation of the two observations. Without additional spacecraft, no further interpretation of a feature's stationarity can be made.

Features in a shock profile which vary on the timescale of the proton gyroperiod could influence the population of solar wind particles that are reflected at the shock front, whereas the instantaneous configuration of the magnetic profile influences the particles which pass directly through the shock ramp. The crossing time for a directly-transmitted ion is roughly $L_{\rm ramp}/V_u \lesssim 1/M_A\Omega_u$ (assuming that $L_{\rm ramp} \lesssim c/\omega_{pi}$), which is generally considerably smaller than the timescale of the profile variations in a shock observation (as we shall show in section 4.2). This quasi-stationarity has implications on the particle dynamics within the shock front: It suggests that the instantaneous configuration of electromagnetic fields governs the motion of ions and electrons transmitted directly through the shock front, whereas analysis of reflected ion motion requires taking slow temporal field variations into account. This may also affect the resulting downstream distribution, which is formed nonlocally.

There is, of course, some subjectivity introduced into the analysis when determining which features (if any) match up. However, it is important to keep in mind that any interpretation, including one based on cross correlation, will have a degree of subjectivity unless the observer has complete spatial and temporal observations, a data set which no mission can provide.

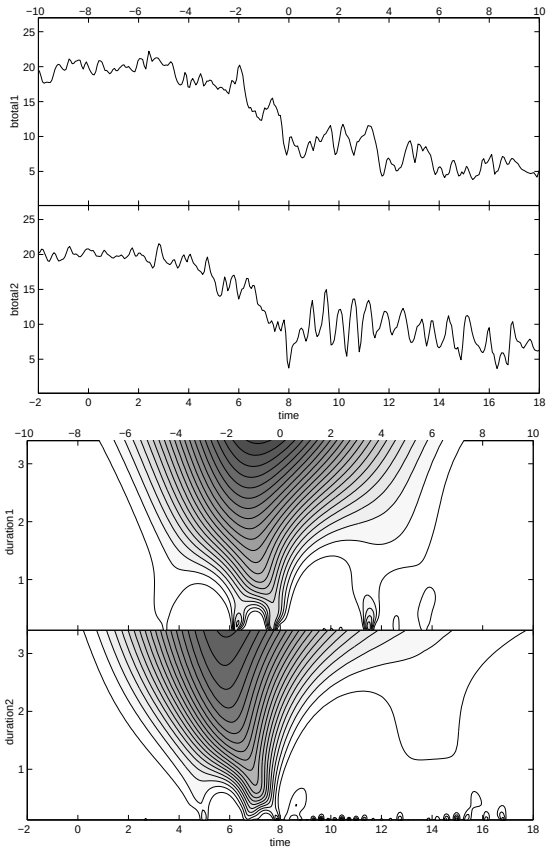

Figure 4. (a) The central 20 s of the August 2, 1980, 0858 UT shock, focusing on the details of the ramp transition (classified as a single transition, or S-type shock ramp). t = 0 corresponds to 0858:50 UT. (b) The g_1 wavelet transform of the above profiles. The wavelet transforms highlight the quasi-stationary subscales in the ramp.

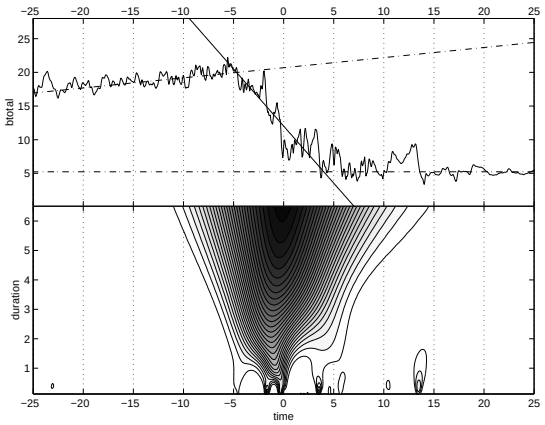

Figure 5. Ramp scale measured with a linear fit (top panel) and based on the g_1 wavelet transform (bottom panel). The linear fit describes the global ramp transition, whereas sharp gradient, large-amplitude scales are emphasized in the wavelet transform (t=0=0858:50 UT on August 2, 1980).

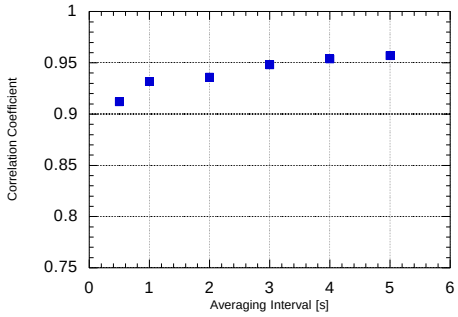

Figure 6. Cross-correlation of the ISEE 1 and 2 $B_{\rm tot}$ profiles for the August 2, 1980, shock as a function of profile averaging interval. The correlation coefficient begins to noticeably decline at intervals less than 1 s.

4. Examples of Ramp Observations

The ramp structures in the shocks listed in Table 1 do not consistently fit the simple, monotonic shock ramp model commonly applied in collisionless shock theory. The observed ramps vary over a wide range of behavior and scale size: Shock ramps may contain a single, stationary subscale within the global ramp, while others are more complex, with several subscales in the global ramp.

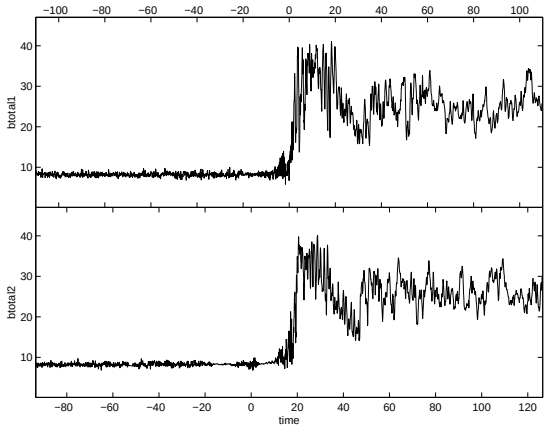

Figure 7. The $B_{\rm tot}$ profiles observed by ISEE 1 (top) and 2 (bottom). This shock was observed on August 4, 1978, and $t = 0$ = 1809:30 UT. $M_{\rm MS} = 3.9$, $\beta = 0.91$, and $\theta_{Bn} = 86^\circ$.

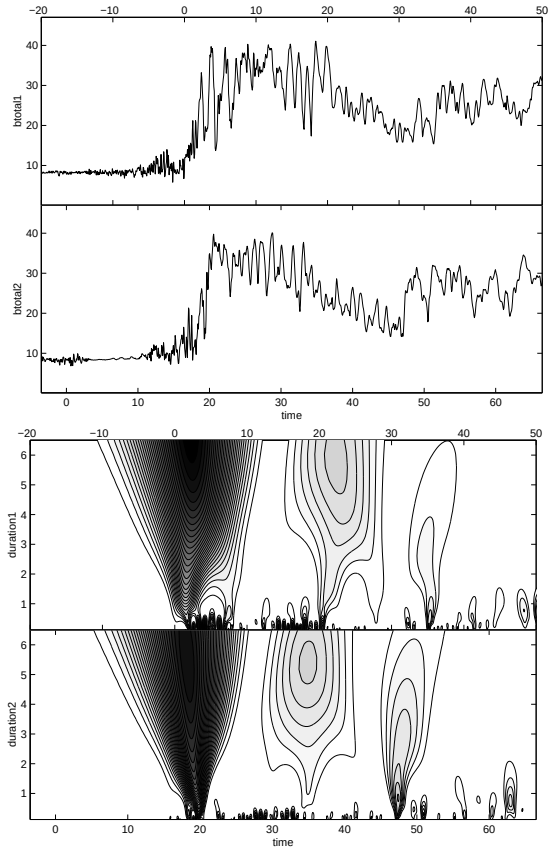

Figure 8. (a) The central 70 s of the August 4, 1978, 1809 UT shock. Despite the similarities in the overall shock profiles, the ramp observations are quite different. This shock is classified as complex, or type C. (b) The g_1 wavelet transforms for the above profiles (t=0=1809:30 UT).

Some shock ramps oscillate with a period on the order of the proton gyroperiod, and other ramps are clearly nonstationary and oscillate with a period much shorter than the gyroperiod. It is not practical to discuss every observation listed in Table 1. Rather, in this section we present four shocks which illustrate four apparent classifications of shock ramp transitions.

4.1. A Shock With a Single Transition

The bow shock observed by ISEE 1 and 2 on August 2, 1980, at 0858 UT is shown in Figure 3. This is a high-Mach-number ($M_{\rm MS} = 3.2$), quasi-perpendicular ($\theta_{Bn} = 86^\circ$), moderate-β ($= 0.62$) shock which exhibits the classic foot-ramp-overshoot profile. The shock ramp is clearly identified in this lengthy 5 min profile, although its finer features are not clear. In Figure 4a, 20 s of this shock is shown, centered about the ramp transition. The ISEE 1 and 2 profiles are matched visually by shifting the ISEE 2 profile by 7.8 s relative to the ISEE 1 magnetic field profile. This time separation corresponds to roughly 0.6 proton gyroperiods, a short enough time to observe the stationary profile. (Temporal variability is expected to be observed when the time separation is substantially larger than the proton gyroperiod.) The spatial separation of the spacecraft along the shock normal is 99 km (= 0.82 c/ω_{pi}), and the shock velocity is +21.5 km/s (directed along the shock normal, or against the incident solar wind flow). The transverse separation of the spacecraft is 101 km (= 0.83 c/ω_{pi}). These spacecraft separations are sufficiently small to assume that large-scale deviations from one-dimensionality (such as shock surface rippling) are not an issue in this case.

Figure 4b displays the g_1 wavelet transforms of the ISEE 1 and 2 profiles in Figure 4a. In Figure 4b it is clearly seen that the only significant feature which can be matched in both profiles is the "local"

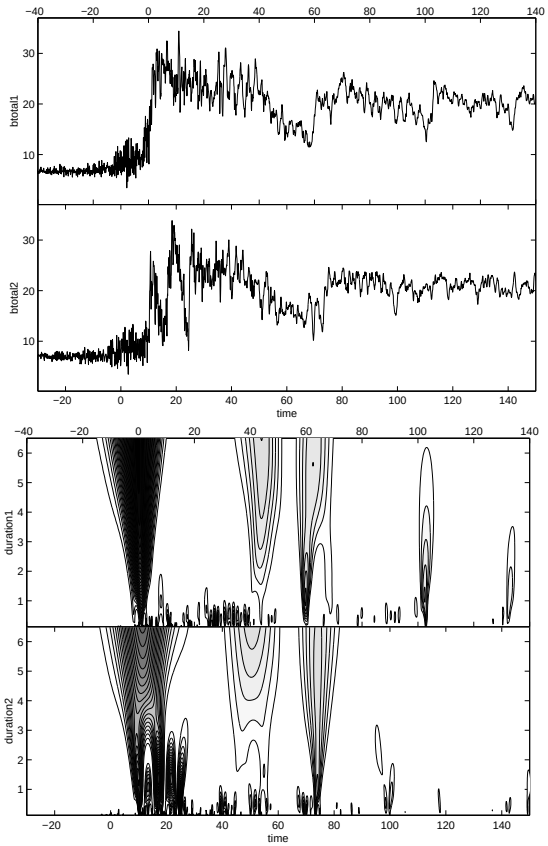

Figure 9. (a) The shock observed on July 23, 1978, 0159 UT. $M_{\rm MS} = 4.4$, $\beta = 1.14$, and $\theta_{Bn} = 72^\circ$. Classified as an oscillating, or type O, shock ramp (t=0=0159:20 UT). (b) The g_1 wavelet transforms for the above profiles.

feature with a duration of 1.5-2 s within the "global" ramp transition. Matching this small-scale feature in the wavelet transforms of the ISEE 1 and 2 profiles yields a separation of approximately 8 s (shown in Figure 4b), which is quite close to the 7.8 s separation determined by a direct visual comparison of the entire shock profile observed by ISEE 1 and 2. This suggests that this local gradient is quasi-stationary (at least within the 7.8 s between shock observations). Other local gradient features (such as those at t = -5 s and t = 3.5 s in the ISEE 1 transform) are observed to change within the time separation.

Figure 7 compares the ramp measurement with a linear fit of the ISEE 1 profile (top panel) to the corresponding wavelet analysis for this interval (bottom panel). In the linear fit the beginning of the ramp transition is defined as the intersection between the linear fit and the upstream magnetic field (lower dotted line). The end of the ramp is defined as the intersection between the linear ramp fit and the linear approximation of the overshoot (upper dotted line). The linear fit characterizes the overall width of the transition, a duration of about 8.1 s (which corresponds to $\sim$0.9 c/ω_{pi}). As seen in the top panel this global ramp interval includes three large, visually distinguishable magnetic field jumps, each of which has an amplitude that is larger than the upstream magnetic field and comparable to the amplitude of the total magnetic field jump. The wavelet transform shows that not all features in this transition are of equal importance, and clearly indicates the main structure. It lasts for slightly less than 2 s (from $t \approx -2$ to $t = 0$), during which time the steep magnetic field gradient is accompanied by a large magnetic field increase (by a factor of 3). The width of this subscale is $\sim$0.2 c/ω_{pi}. In Figure 4b this scale can also be clearly seen in the wavelet transform of the ISEE 2 data, which allows us to conclude with confidence that this feature is a part of the stationary shock structure. It is tempting to interpret the two successive jumps in the magnetic profile of Figure 7 as separate substructures, a hypothesis which is supported by the ISEE 1 wavelet transform panel. However, the ISEE 2 wavelet transform does not highlight these jumps. Therefore it is more likely that the transition is distorted by a large amplitude wave crossing the ramp or is weakly nonstationary.

A more standard approach to investigating the stationarity of features within a profile is to cross correlate the multispacecraft observations, after the profiles have been averaged over a series of different time increments (see *Scudder et al.* [1986a] Figure 9). Figure 8 presents such an analysis for the August 2, 1980, shock, showing the correlation coefficient as a function of the averaging interval. For this shock, correlation begins to decline for intervals less than 1 s, suggesting that the the magnetic profile may not be one-dimensional and/or stationary for shorter time intervals. This conclusion can also be reached by examining the g_1 wavelet transforms in Figure 3b. The contours converging from large durations become disturbed and broken for wavelet durations less than 1 s. The subramp scale identified above has a duration of 1.7 s.

4.2. A Shock With a Complex Transition

Figure 5 contains the ISEE 1 and 2 profiles from another high-Mach-number shock. At first glance this shock appears to be a "well-behaved," classic example of a bow shock, but in fact it is quite complex. This shock, observed on August 4, 1978, at 1809 UT, has the following parameters: $M_{\rm MS} = 4.0$, $\theta_{Bn} = 63^\circ$, and $\beta = 0.87$. The shock velocity is 11.9 km/s, based on a normal separation of 202 km (= 2.21 c/ω_{pi}) and a time separation of 16.6 s (= 2.08 proton gyroperiods). The transverse separation is 2.16 c/ω_{pi}. On the basis of this figure, it appears that it would be possible to confidently determine the ramp position and width. However, the ramp appears to be more complicated when we zoom in upon the ramp feature. The central 70 s of the profile is shown in Figure 6a where very different substructure is evident in the ISEE 1 and 2 ramps. In this case the spacecraft time separation is large enough to witness the shock variability at the proton gyroperiod scale. It should be understood that the two spacecraft measurements do not allow one to conclude unambiguously whether temporal variations or spatial variations along the shock front are observed and that some assumptions must be invoked. The spatial separation along the shock front is slightly larger than in the previous case, but it is still small enough to reasonably to assume that the ISEE 1 and 2 spacecraft are observing the time variability of the same piece of a one-dimensional shock.

The overall structure of the shock is remarkably stable, which can be seen in the large-scale similarities between the wavelet transforms of the ISEE 1 and 2 profiles (Figure 6b). The three main features in each transform retain their relative positions (within 2 s) during the 16.6 s separating the ISEE 1 and 2 observations. The time between these features is slightly shorter for ISEE 2 than for ISEE 1, which suggests that the two downstream structures slowly approach the shock ramp or that the shock has accelerated slightly during this period. We match the first two rising slopes in the main ramp transition of the ISEE 1 profile to the two rising slopes of the ISEE 2 ramp, and conclude that the third slope in the ISEE 1 profile overtakes and merges with the previous ones during the two gyroperiods of time separating the spacecraft observations. Notice that the second slope continues to steepen. It is also worth mentioning that the wavelet transform shows a second large scale of $\sim$8 s duration in the ISEE 1 profile, which covers all steep, large-amplitude gradients within the ramp transition. This scale does not exist for the ISEE 2 profile, and we attribute this difference to the overtaking of this scale by the downstream plasma and magnetic field accompanied by the steepening of the slopes within the ramp. It is essential that this process is slow and that the first slope is not absorbed by the profile coming from behind. The crossing time for a proton which passes directly through the shock is $L_{\rm ramp}/V_u \lesssim 1/M_A\Omega_u = 0.25$ s, considerably smaller than the timescale of the profile variation. Thus, we may consider the shock to be approximately stationary (within a proton gyroperiod) and estimate the smallest scale of the ramp as $\sim$0.15 c/ω_{pi} ($\approx$ 1 s duration).

4.3. An Oscillating Shock Ramp

The shock observed on July 23, 1978, at 0159 UT represents a third classification: one in which the ramp appears to oscillate. This is another high-Mach-number, high-β, quasi-perpendicular shock ($M_{\rm MS}$ = 4.4, β =1.14, θ_{Bn} = 72°). The ISEE 1 and 2 profiles, shown in Figure 9a, appear quite different at the ramp. The ISEE 1 profile has a single, sharp, well-defined ramp transition, whereas the ISEE 2 profile contains three distinct transitions, each with a similar amplitude. The time separation between the two spacecraft is not large (16 s = 1.6 proton gyroperiods), but the transverse spatial separation is significant (= 5.9 $c/\omega_{pi} \approx V_u/\Omega_u$). This suggests that in this case there is spatial variability of the shock's fine structure along the shock surface at this scale. This also suggests that the motion of reflected ions is likely to be sensitive to the

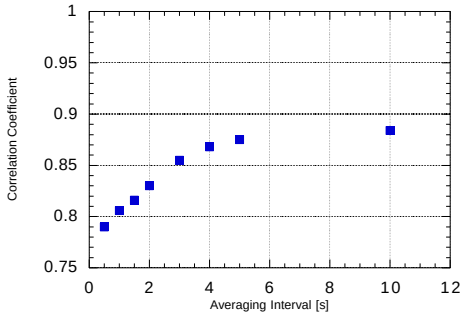

Figure 10. The cross-correlation of the ISEE 1 and 2 $B_{\rm tot}$ profiles for the July 23, 1978, shock as a function of a profile averaging interval. The correlation coefficient begins to noticeably decline at intervals less than 5 s.

three-dimensional structure of the shock front, and a simple one-dimensional model may not be applicable. Matching the overall shock profiles observed by ISEE 1 and 2 results in a shock velocity of 9.0 km/s.

The ISEE 1 and 2 profiles exhibit secondary fronts downstream, which suggests using the same procedure as in the previous example (section 4.2). Figure 9b contains the g_1 wavelet transforms for these two profiles. If we identify the three distinct ISEE 1 features (near $t = 0$ s, $t = 60$ s, and $t = 100$ s) with the three ISEE 2 features (near $t = 10$ s, $t = 70$ s, and $t = 95$ s), we see that their relative positions are fairly stable, despite the substantial time separation between the ISEE 1 and 2 measurements. We conclude that the overall profile is quasi-stationary except in the ramp itself, which appears to be oscillating.

The scale size of the ramp can be estimated from the ISEE 2 profile. Roughly assuming that the front oscillates in the shock frame symmetrically, the average velocity of the front is $v_{\rm osc} \pm v_{\rm sh}$, where $v_{\rm osc}$ is the average velocity of the oscillations. The rising upstream-to-downstream gradient is crossed in $\tau_1 \approx 1.25$ s, and the decreasing downstream-to-upstream gradient is crossed in $\tau_2 \approx 5$ s. This yields:

$$L = (v_{\rm osc} + v_{\rm sh})\tau_1 = (v_{\rm osc} - v_{\rm sh})\tau_2 \quad (5)$$

Solving for $v_{\rm osc}$ and then for L:

$$v_{\rm osc} = v_{\rm sh}\frac{\tau_2 + \tau_1}{\tau_2 - \tau_1} = \frac{3}{2}v_{\rm sh}, \quad (6)$$

$$L = v_{\rm sh}\frac{2\tau_1\tau_2}{\tau_2 - \tau_1} = \frac{5}{2}v_{\rm sh}\tau_1 \quad (7)$$

Equation (7) shows that the width of the slope can be calculated according to the effective duration. This results in an estimate of 0.33 c/ω_{pi} for the upper limit of the scale size of the steepest gradient with the largest magnetic field jump.

Following the cross-correlation procedure in section 4.1, Figure 10 contains a plot of the cross-correlation coefficient as a function of profile averaging intervals. The correlation between the ISEE 1 and 2 profiles is seen to decline for intervals less than 5 s, the period of the oscillating ramp. The g_1 wavelet transform suggests that scales less than $\sim$ 4 s are nonstationary in the ISEE 2 profile. Our estimate of 0.33 c/ω_{pi} (= 3.1 s) for the upper limit of the scale size of the steepest gradient with the largest magnetic field jump is less than either of these limits on "stationarity." However, as this value was determined on the basis of the assumption of an oscillating ramp, we make no pretenses as to its stationarity.

In this particular case not only are the solar wind particles moving through a sharp transition but the transition itself is oscillating with a period of $T \approx \tau_1 + \tau_2 \approx 6s$, which is slightly less than the ion gyroperiod ($= 9.9s$). The wavelength of these oscillations is $\Delta x \approx V_{osc}T \sim c/\omega_{pi}$. These oscillations would result in efficient smoothing of the downstream distribution of directly transmitted ions and electrons, even though the local dynamics of these particles in the ramp should not be sensitive to these variations. This oscillatory behavior could substantially change the ion reflection process at the shock front.

4.4. A Nonstationary Shock

In the previous section the shock profile was weakly nonstationary, changing slowly in comparison to the gyroperiod timescale. Our final example is clearly nonstationary, since it contains large-amplitude oscillations with periods that are much faster than the proton gyroperiod.

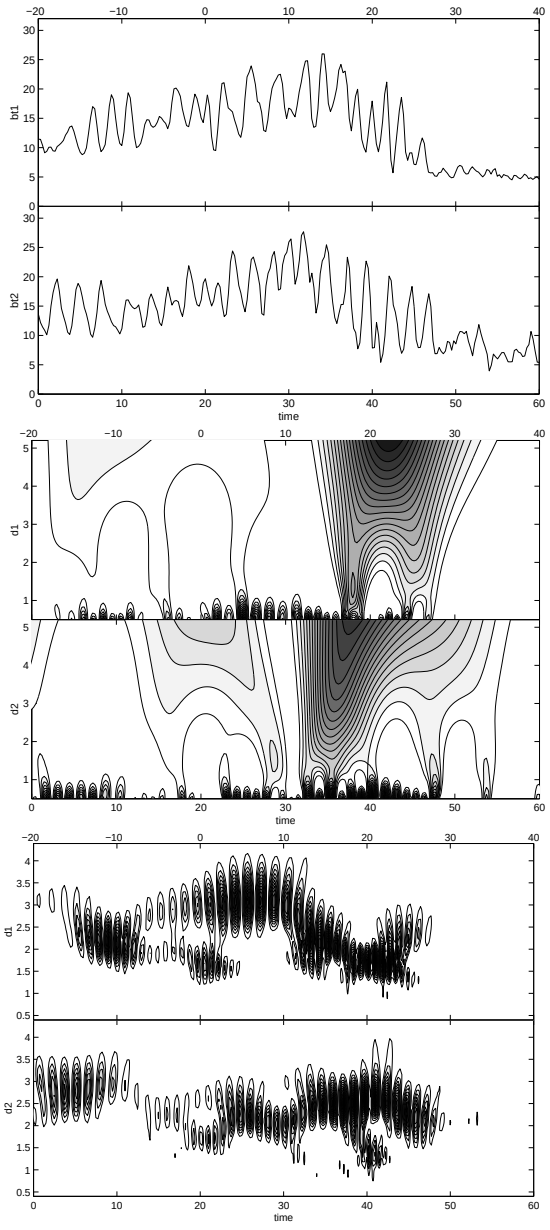

Figure 11. (a) ISEE 1 and 2 $B_{\rm tot}$ profiles for the December 20, 1977, 1609 UT shock (t=0=1608:40 UT, $M_{\rm MS} = 4.1$, $\beta = 2.44$, and $\theta_{Bn} = 77^\circ$). This is a nonstationary, or type N, shock ramp. (b) The g_1 transforms and (c) m transforms of the above profiles. The m transform highlights periodic structures, here with periods of 2-4 s (proton gyroperiod = 15.2 s). The transforms match when shifted by 0.8-1.1 s, suggesting the waves are convected downstream at $\sim v_{sw}$.

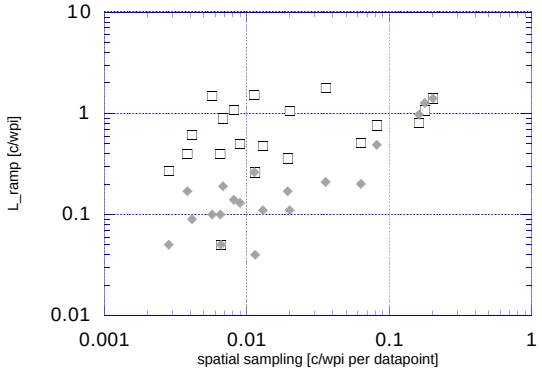

Figure 12. Ramp width versus spatial sampling of the shock profile by the ISEE spacecraft. Open squares indicate $L_{\rm ramp}$ and solid diamonds indicate $L_{\rm sub}$. Coarse sampling does not accurately resolve the fine $L_{\rm sub}$ scales.

Our final example was observed on December 20, 1977, at 1609 UT and is characterized by the following parameters: $M_{\rm MS} = 2.8$, $\theta_{Bn} = 78^\circ$, and $\beta = 2.49$. Figure 11a contains the ISEE 1 and 2 profiles for this shock. With oscillations of such magnitude on the ramp there is no clear way to determine the ramp position and width. On the basis of a visual comparison of the two profiles, the shock velocity is estimated to be -7.5 km/s (SC separations normal and transverse are 150 km = 1.8 c/ω_{pi} and 281 km = 3.4 c/ω_{pi}; time separation $\approx$ 20s $\approx$ the proton gyroperiod). Figure 11b shows that the transition covers roughly 20 s of measurements, but all slopes within the transition are on the same order of magnitude in both scale and amplitude, rendering the approach from section 4.3 useless in this case.

For this shock a study of the wave activity through the Morlet wavelet transform (Figure 11c) may be informative [*Gedalin et al.*, 1998]. The shock transition layer is characterized by a long, large-amplitude wave train with a period of 2-4 s. The ISEE 1 and 2 Morlet transforms of these waves are quite similar, and match up almost exactly when shifted by 0.8-1.1 s (and not the 20 s shift required to match up the shock fronts). This is roughly the time taken by the solar wind to travel the distance separating the two spacecraft, suggesting that these waves are being convected downstream at that speed. The Morlet transform does not provide any further information about ramp scale sizes. The oscillation period is substantially smaller than the proton gyroperiod (= 15.2 s) indicating the nonstationary nature of this shock front: Any definitive conclusions based on the observations are impossible with the present status of theory.

5. Shock Analysis Statistics

As we have seen in the previous section there does not appear to be a single typical profile for a high-Mach-number shock if its fine structure is taken into account. We have seen that in a number of cases this fine structure is quasi-stationary. In other cases it may be oscillating; in yet another case the fine structure is nonstationary and no confident conclusions can be made regarding the nature of the shock's structure. However, in all of these cases the observed substructures in the ramp have amplitudes which are comparable to the overall jump in the magnetic field and should be considered as parts of the shock structure rather than superimposed wave activity. With this is mind, we suggest the following phenomenological classification of high-Mach-number shocks listed in Table 1 according to their fine structure: "S" denotes shocks with a single, nearly monotonic ramp transition (such as the August 2, 1980, shock: see section 4.1 and Figure 4a); "C" denotes shocks with complex, multipart ramp transitions which can be considered quasi-stationary on the proton gyroperiod timescale (such as the August 4, 1978, 1809 UT shock: see section 4.2 and Figure 6a); "O" denotes shocks with an apparent single, oscillating ramp (see the July 23, 1978, shock: see section 4.3 and Figure 9a); and "N" denotes shocks with an unidentifiable ramp in which the wide, overall transition from upstream to downstream consists of a number of large amplitude formations (such as the December 20, 1977, 1608 UT shock: see section 4.4 and Figure 11a). We do not claim that this classification is complete, nor do we claim that every shock can be reliably attributed to one of these classes. However, by taking into account the variety of high-Mach-number shocks that we have encountered in the ISEE data set and the apparent absence of a typical, universal ramp profile, we consider this classification to be a first attempt to identify several basic types of supercritical shock behavior.

Table 3 lists the shocks in Table 1 according to this classification, along with several derived parameters. The shock velocity is expressed in terms of ion inertial lengths per second. The global ramp width $L_{\rm ramp}$ is determined by the simple linear fit of the entire transition. As a rule, $L_{\rm ramp}$ covers all substructure within the ramp, including as many as 10 periods of large-amplitude magnetic field variations in type N shocks. The steep-gradient subscales, $L_{\rm sub}$, are determined by measuring the duration of the steepest magnetic field increase within the ramp, provided the amplitude of this increase is comparable to the overall magnetic field jump at the ramp (as indicated by the g_1 wavelet transform). The duration Δt of a feature is converted into a spatial-scale ΔL using the stationary relationship $\Delta L = v_{\rm sh}\Delta t$ in all cases, although this may be misleading in O- and N-type shocks where the assumption of constant $v_{\rm sh}$ may not be valid. The scale lengths are expressed in terms of ion inertial length which is more physically meaningful than dimensional units. In Table 3 the final column indicates the observation's resolution: "H" indicates high-resolution (16 magnetic field vectors/s), and "L" indicates low (4 vectors/s).

The typical length of subscale gradients within the global ramp is $\sim$0.1-0.2 c/ω_{pi}, independent of the shock type. It is substantially smaller than the global ramp width, which suggests that the ramp transition is often significantly structured. In the four cases where the gradient scale is comparable in size to the ramp width and substantially exceeds 0.1-0.2 c/ω_{pi}, the shock velocity is high and the data resolution is low. In three cases the shock velocity is on the order of $(c/\omega_{pi})/s$, and the observed absence of the ramp structure may simply be due to insufficient data resolution.

This effect is also seen in Figure 12, where the ramp scales are plotted as a function of the spatial sampling of the shock profile by the ISEE spacecraft (i.e., shock velocity/data resolution). The thinnest scales are resolved when the spatial sampling of the profile by the spacecraft is very small. When sampling is coarse ($\geq$0.1 c/ω_{pi}), $L_{\rm sub}$ is larger. $L_{\rm ramp}$ is not affected by the spatial sampling of the shock front for this selection of shock observations; its scale is large enough to be consistently resolved by the spacecraft.

It should be stressed that the spatial representation of the ramp scales (both large and small) is for convenience. The only available dimensionless parameter is $v_{\rm sh}\Delta t/(c/\omega_{pi})$, where Δt is the

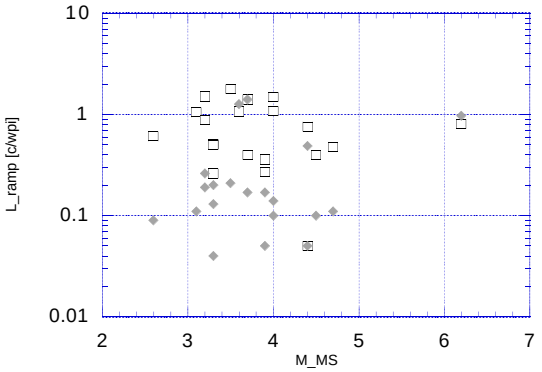

Figure 13. Ramp width versus upstream magnetosonic Mach number. Open squares indicate $L_{\rm ramp}$ and solid diamonds indicate $L_{\rm sub}$. There is no trend between ramp scale and Mach number. (Cases where $L_{\rm ramp} \approx L_{\rm sub} \approx c/\omega_{pi}$ are high velocity shocks.)

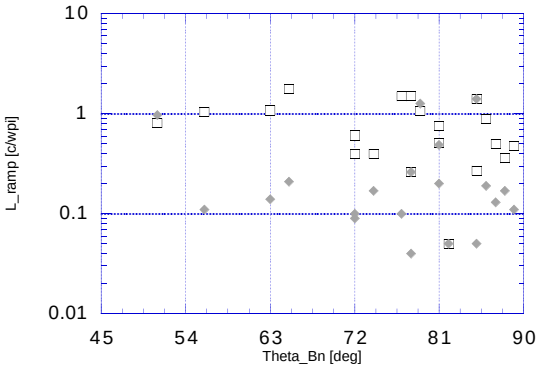

Figure 14. Ramp width versus upstream θ_{Bn}. Open squares indicate $L_{\rm ramp}$ and solid diamonds indicate $L_{\rm sub}$. As θ_{Bn} approaches 90°, there is a thinning of the global ramp width.

duration of the feature in question. For stationary shocks this is the correct spatial scale. For clearly nonstationary shocks we do not have another way to make a qualitative comparison, so we use the same measure.

Finally, we have investigated the dependence of the ramp scales on the upstream plasma parameters. In Figure 13 the ramp width and gradient scale are plotted versus magnetosonic Mach number. There is no clear dependence between the scales and Mach number. A plot of scale sizes versus β shows the same lack of an overall trend. However, in Figure 14, we can see a decrease in $L_{\rm ramp}$ as θ_{Bn} approaches 90°, although certainly not the dramatic $c\cos\theta_{Bn}/\omega_{pi}$ trend predicted by *Kennel and Sagdeev* [1967]. Comparison between Table 1 and Table 3 shows no correlation between shock ramp complexity and upstream parameters.

6. Conclusions

We have investigated the ramp structures observed in a variety of quasi-perpendicular, high-Mach-number bow shocks observed by the ISEE spacecraft. We have found that the width of the overall ramp transition (based on a linear fit of the total magnetic field profile from the foot to overshoot) is typically within the range 0.5-1.5 c/ω_{pi}. The ramp transition does not conform to a single model: It can be a single, narrow, nearly monotonic ramp, or it can be a wide layer containing as many as 10 large oscillations with amplitudes comparable to the overall magnetic field jump. We have found that in most cases the ramp transition can be characterized by two distinct scales: (1) the large global ramp scale, which corresponds to the main transition between upstream and downstream field conditions and contains all substructure, and (2) the smaller subramp scale, which corresponds to steep gradient, large-amplitude features within the global ramp. In a number of shocks, we have shown that these steep subramp features are quasi-stationary (or slowly time-varying with respect to the gyroperiod) and that their typical spatial scales are generally 0.1-0.2 c/ω_{pi}. In one case where the ramp was clearly oscillating we were able to estimate the velocity of oscillations and corresponding scale, which was approximately in the same range as above. We conclude therefore that these scale sizes are typical for high-Mach-number, quasi-perpendicular shocks, unless the shock profile changes on a timescale substantially smaller than the proton gyroperiod. In this case the shock is nonstationary from the point of view of the incident solar wind plasma; any interpretation of the shock front as a stationary and one-dimensional structure would be incorrect and misleading.

Since the amplitude of these steep, subramp features is comparable to the overall magnetic field jump, they should be considered as parts of the shock structure (independently of whether they are stationary or time varying) and not as superimposed wave activity. The motion of ions and electrons which are directly transmitted through the ramp is governed by the instantaneous field configuration and not the average field structure since the time for a particle to cross through the ramp is much smaller than the timescale of the field variation. The small-scale substructure may play an important role in the formation of the downstream ion distribution by providing efficient ion scattering in phase space and preventing strong quasi-periodic ion bunching, which is typical for static monotonic transitions [*Zilbersher et al.*, 1998]. This smoothing of the ion distribution by quasi-stationary fields may be essential for shock stability. The small-scale substructure may also significantly alter the ion reflection process, which occurs in the tail of the incident ion distribution [*Burgess et al.*, 1989] and thus may be sensitive to these inhomogeneities. Additional complications may be introduced by the clear nonstationarity of the shock profile in some cases and by the three-dimensional rippling of the shock surface. In such cases, reflected ions essentially interact with different transition layers during their multiple encounters with the shock ramp. In one case, we have been able to successfully determine the scale ($\sim v_u/\Omega_u$) of this rippling, due to the favorable configuration of the ISEE 1 and 2 spacecraft.

We have found that shock observations with no substructure can be explained in terms of coarse spatial sampling of the profile due to high shock velocity. When the shock front has a low velocity, fine-scale structure (0.1-0.2 c/ω_{pi}) on the ramp is consistently observed. Future multispacecraft missions to study the bow shock will need to have a high time resolution of 20 Hz or more and close spatial separations of a few c/ω_{pi} (under $\sim$200 km) in order to address the questions associated with shock structure. The Cluster mission can provide the required temporal resolution [*Balogh et al.*, 1997], but the planned separation strategy concentrates on distances much greater than 200 km [*Escoubet et al.*, 1997].

Acknowledgments. The wavelet transforms were calculated using the WaveLab package for Matlab. This research was supported by the National Science Foundation under grant ATM 94-13081 and by grant 94-00047 from the United States-Israel Binational Science Foundation (BSF), Jerusalem, Israel.

The Editor thanks the referees for their assistance in evaluating this paper.

References

Balogh, A., et al., The Cluster magnetic field investigation, *Space Sci. Rev., 79*, 65-91, 1997.

Bame, S. J., J. R. Asbridge, H. E. Felthauser, J. P. Glore, G. Paschmann, P. Hemmerich, K. Lehmann, and H. Rosenbauer, ISEE 1 and 2 fast plasma experiment and the ISEE 1 solar wind experiment, *IEEE Trans. Geosci. Electron., 16*, 216-220, 1978.

Burgess, D., W. P. Wilkinson, and S. J. Schwartz, Ion distributions and thermalization at perpendicular and quasi-perpendicular supercritical collisionless shocks, *J. Geophys. Res., 94,* 8783-8792, 1989.

Escoubet, C. P., R. Schmidt, and M. L. Goldstein, Cluster-Science and mission overview, *Space Sci. Rev., 79*, 11-32, 1997.

Farge, M., Wavelet transforms and their applications to turbulence, *Ann. Rev. Fluid Mech., 24*, 395-457, 1992.

Farris, M. H., S. M. Petrinec, and C. T. Russell, The thickness of the magnetosheath: Constraints on the polytropic index, *Geophys. Res. Lett., 18,* 1821-1824, 1991.

Farris, M. H., C. T. Russell, and M. F. Thomsen, Magnetic structure of the low beta, quasi-perpendicular shock, *J. Geophys. Res., 98,* 15,285-15,294, 1993.

Feldman, W. C., Electron velocity distributions near collisionless shocks, in *Collisionless Shocks in the Heliosphere: Reviews of Current Research, Geophys. Monogr. Ser.,* vol. 35, edited by R. G. Stone and B. T. Tsurutani, pp. 195-205, AGU, Washington, D. C., 1985.

Galeev, A., V. Krasnosel'skikh, and V. Lobzin, Fine structure of the front of a quasi-perpendicular supercritical collisionless shock wave, *Sov. J. Plasma Phys., 14,* 697-702, 1988.

Gedalin M., Ion reflection at the shock front revisited, *J. Geophys. Res., 101,* 4871-4878, 1996.

Gedalin, M., J. A. Newbury, and C. T. Russell, Shock profile analysis using wavelet transforms, *J. Geophys. Res., 103*, 6503-6512, 1998.

Greenstadt, E. W., C. T. Russell, F. L. Scarf, V. Formisano, and M. Neugebauer, Structure of the quasi-perpendicular laminar bow shock, *J. Geophys. Res., 80,* 502-514, 1975.

Kennel, C. F., and R. Z. Sagdeev, Collisionless shock waves in high β plasmas, 1, *J. Geophys. Res., 72,* 3303, 1967.

Karpman, V. I., Structure of the shock front propagating at an angle of the magnetic field in a low density plasma, *Sov. Phys. Tech. Phys., Engl. Transl., 8*, 715-719, 1964.

Mellott, M. M., and E. W. Greenstadt, The structure of oblique subcritical bow shocks: ISEE 1 and 2 observations, *J. Geophys. Res., 89,* 2151-2161, 1984.

Morse, D. L., and E. W. Greenstadt, Thickness of magnetic structures associated with the earth's bow shock, *J. Geophys. Res., 81,* 1791-1793, 1976.

Newbury, J. A., and C. T. Russell, Observations of a very thin collisionless shock, *Geophys. Res. Lett., 23,* 781-784, 1996.

Newbury, J. A., C. T. Russell, and M. Gedalin, The determination of shock ramp width using the noncoplanar magnetic field component, *Geophys. Res. Lett., 24,* 1975-1978, 1997.

Newbury, J. A., C. T. Russell, J. L. Phillips, S. P. Gary Electron temperature in the ambient solar wind: Typical properties and a lower bound at 1 AU, *J. Geophys. Res., 103,* 9553-9566, 1998.

Rezeau, L., G. Belmont, F. Reberac, Detection of localised structures from multispacecraft data: Adaptive correlation function, *J. Geophys. Res., 103*, 2319-2325, 1998.

Russell, C. T., The ISEE 1 and 2 fluxgate magnetometers, *IEEE Trans. Geosci. Electron., 16*, 239-242, 1978.

Russell, C. T., and E. W. Greenstadt, Initial ISEE magnetometer results: Shock observations, *Space Sci. Rev., 23,* 3-37, 1979.

Sagdeev, R. Z., Cooperative phenomena and shock waves in collisionless plasmas, *Rev. Plasma Phys., 4,* 23, 1966.

Schwartz, S. J., M. F. Thomsen, S. J. Bame, and J. Stansberry, Electron heating and the potential jump across fast mode shocks, *J. Geophys. Res., , 93,* 12923-12931, 1988.

Sckopke, N., G. Paschmann, S. J. Bame, J. T. Gosling, and C. T. Russell, Evolution of ion distributions across the nearly perpendicular bow shock: Specularly and nonspecularly reflected-gyrating ions, *J. Geophys. Res., 88,* 6121-6136, 1983.

Scudder, J. D., A. Mangeney, C. Lacombe, C. C. Harvey, T. L. Aggson, R. R. Anderson, J. T. Gosling, G. Paschmann, and C. T. Russell, The resolved layer of a collisionless, high β, supercritical, quasi-perpendicular shock wave, 1, Rankine-Hugoniot geometry, currents, and stationarity, *J. Geophys. Res., 91,* 11,019-11,052, 1986a.

Scudder, J. D., A. Mangeney, C. Lacombe, C. C. Harvey, and T. L. Aggson, The resolved layer of a collisionless, high β, supercritical, quasi-perpendicular shock wave, 2, Dissipative fluid electrodynamics, and stationarity, *J. Geophys. Res., 91,* 11,053-11,073, 1986b.

Scudder, J. D., A. Mangeney, C. Lacombe, C. C. Harvey, C. S. Wu, and R. R. Anderson, The resolved layer of a collisionless, high β, supercritical, quasi-perpendicular shock wave, 3, Vlasov electrodynamics, *J. Geophys. Res., 91,* 11,075-11,097, 1986c.

Thomsen, M. F., M. M. Mellott, J. A. Stansberry, S. J. Bame, J. T. Gosling, and C. T. Russell, Strong electron heating at the Earth's bow shock, *J. Geophys. Res., 92,* 10,119-10,124, 1987.

Wilkinson, W. P., and S. J. Schwartz, Parametric dependence of the density of specularly reflected ions at quasi-perpendicular collisionless shocks, *Planet. Space Sci., 38,* 419-435, 1990.

Zilbersher, D., M. Gedalin, J. A. Newbury, and C. T. Russell, Direct numerical testing of a stationary shock model with low Mach number shock observations, *J. Geophys. Res.,* in press, 1998.

Table 1. Shock Parameters

Date, Time (UT)	$M_{\rm MS}$	M_A	θ_{Bn}, deg	β	β_p	$2\pi/\Omega_p$, s	c/ω_{pi}, km
Nov. 30, 1977, 0621	3.3	5.0	78	1.64	0.52	5.98	43.5
Nov. 30, 1977, 0636	3.3	4.8	81	1.39	0.43	5.60	43.9
Nov. 30, 1977, 2231	6.2	9.8	51	2.18	0.32	10.72	60.3
Dec. 15, 1977, 2016	3.5	6.4	65	2.24	0.48	17.13	99.3
Dec. 20, 1977, 1549	3.9	6.0	85	1.69	0.28	12.26	79.3
Dec. 20, 1977, 1609	4.0	6.9	77	2.44	0.35	15.22	82.0
Dec. 20, 1977, 1619	3.7	6.0	74	2.13	0.33	15.12	86.5
Dec. 20, 1977, 1732	3.3	6.0	87	2.62	0.35	14.58	74.3
Jan. 6, 1978, 0701	3.1	3.3	56	0.25	0.05	4.79	83.7
July 23, 1978, 0159	4.5	6.3	72	1.14	0.36	9.88	85.9
Aug. 4, 1978, 1652	2.6	3.4	72	0.94	0.46	7.98	89.1
Aug. 4, 1978, 1809	4.0	5.1	63	0.87	0.41	7.98	91.2
July 16, 1979, 1646	3.2	5.5	78	2.49	1.16	11.08	83.0
Aug. 13, 1979, 1426	3.6	3.8	79	0.10	0.05	2.62	62.4
July 11, 1980, 1356	3.7	4.2	85	0.34	0.06	5.76	80.7
Aug. 1, 1980, 2135	4.4	6.1	82	0.93	0.19	18.51	136.2
Aug. 2, 1980, 0858	3.2	4.0	86	0.62	0.21	12.51	121.2
Aug. 9, 1980, 1516	4.4	5.7	81	0.78	0.12	8.84	65.0
Dec. 12, 1980, 0754	4.7	5.0	89	0.14	0.03	4.94	132.5
Dec. 12, 1980, 0806	3.9	4.1	88	0.18	0.06	5.06	121.3

Table 2. Spacecraft Separations and Shock Velocity

Date, Time (UT)	ISEE 1 Location, GSE (R_E)	SC separation, GSE, km	$\Delta d_{\mathrm{SC,n}}$, km	$\Delta d_{\mathrm{SC,t}}$, km	$v_{\mathrm{sh,n}}$, km/s
Nov. 30, 1977, 0621	(1.578, -14,199, 5.810)	(-107.6, 304.8, -185.9)	350	128	-2.0
Nov. 30, 1977, 0636	(1.700, -14.374, 5.906)	(-106.0, 297.0, -182.9)	345	116	+11.1
Nov. 30, 1977, 2231	(9.149, -8.339, 5.252)	(190.1, -454.4, 200.6)	409	339	+39.0
Dec. 15, 1977, 2016	(6.267, -17.677, 8.196)	(-23.1, -260.7, 69.7)	157	221	-14.2
Dec. 20, 1977, 1549	(4.977, -17.780, 7.999)	(-49.1, -293.1, 86.9)	143	275	+3.6
Dec. 20, 1977, 1609	(5.037, -17.630, 7.940)	(-48.2, -301.3, 91.1)	150	281	7.5
Dec. 20, 1977, 1619	(5.072, -17.542, 7.899)	(-47.6, -306.4, 93.5)	192	261	+5.3
Dec. 20, 1977, 1732	(5.288, -16.925, 7.640)	(-43.2, -337.8, 110.0)	240	266	-10.7
Jan. 6, 1978, 0701	(-1.036, -19.302, 8.234)	(-148.5, -251.8, 71.1)	116	278	+6.7
July 23, 1978, 0159	(8.460, 19.124, 7.167)	(-322.0, 408.5, -97.3)	144	509	+9.0
Aug. 4, 1978, 1652	(7.450, 17.863, 5.111)	(-241.8, 32.6, -139.4)	244	140	+5.9
Aug. 4, 1978, 1809	(6.881, 17.510, 4.824)	(-244.4, 8.175, -140.9)	202	197	+11.9
July 16, 1979, 1646	(5.051, 21.287, 3.544)	(327.5, -295.2, 54.3)	67	439	-15.0
Aug. 13, 1979, 1426	(11.196, 6.212, 4.253)	(-592.3, -599.9, -273.0)	756	462	+44.5
July 11, 1980, 1356	(3.722, -21.657, 0.564)	(33.5, -12.7, 21.6)	33	26	+65.3
Aug. 1, 1980, 2135	(11.731, 17.517, 1.115)	(36.5, -146.5, 57.5)	48	154	+3.6
Aug. 2, 1980, 0858	(9.446, 19.872, -0.698)	(124.1, 5.8, 63.3)	99	101	-13.2
Aug. 9, 1980, 1516	(11.028, 18.579, -1.093)	(128.1, 7.572, 58.696)	107	92	-21.5
Dec. 12, 1980, 0754	(10.285, -14.355, -3.157)	(30.1, -314.9, 35.4)	184	259	+27.5
Dec. 12, 1980, 0806	(10.269, -14.210, -3.170)	(33.2, -319.3, 34.5)	207	248	-37.6

Table 3. Ramp Widths

Date, Time (UT)	Type	$V_{\mathrm{sh,n}}$, c/ω_{pi}/s	L_{ramp}, c/ω_{pi}	L_{sub}, c/ω_{pi}	Resolution
Nov. 30, 1977, 0621	S(?)	0.05	0.26	0.04	L
Nov. 30, 1977, 0636	S	0.25	0.51	0.20	L
Nov. 30, 1977, 2231	S	0.65	0.81	0.97	L
Dec. 15, 1977, 2016	S	0.14	1.79	0.21	L
Dec. 20, 1977, 1549	N(?)	0.05	0.27	0.05	H
Dec. 20, 1977, 1609	N	0.12	1.50	0.10	H
Dec. 20, 1977, 1619	N	0.06	0.40	0.17	H
Dec. 20, 1977, 1732	N(?)	0.14	0.50	0.13	H
Jan. 6, 1978, 0701	C(?)	0.08	1.05	0.11	L
July 23, 1978, 0159	O	0.10	0.40	0.10	H
Aug. 4, 1978, 1652	C(N)	0.07	0.61	0.09	H
Aug. 4, 1978, 1809	C	0.13	1.08	0.14	H
July 16, 1979, 1646	C(N)	0.06	0.55	0.09	H
Aug. 13, 1979, 1426	S	0.71	1.07	1.26	L
July 11, 1980, 1356	S	0.81	1.41	1.41	L
Aug. 1, 1980, 2135	S	0.03	0.05	0.05	H
Aug. 2, 1980, 0858	S	0.11	0.89	0.19	H
Aug. 9, 1980, 1516	S	0.33	0.76	0.49	L
Dec. 12, 1980, 0754	S(C)	0.21	0.48	0.11	H
Dec. 12, 1980, 0806	S	0.31	0.36	0.17	H